PHOTONICS Research

Nonlinear photonics with metasurfaces

POLINA VABISHCHEVICH[1,2,4] AND YURI KIVSHAR[3,*]

[1]Physical Measurement Laboratory, National Institute of Standards and Technology, Gaithersburg, Maryland 20899, USA
[2]Department of Chemistry and Biochemistry, University of Maryland, College Park, Maryland 20742, USA
[3]Nonlinear Physics Center, Research School of Physics, Australian National University, Canberra ACT 2601, Australia
[4]e-mail: polina.vabishchevich@nist.gov
*Corresponding author: yuri.kivshar@anu.edu.au

Received 14 September 2022; revised 16 November 2022; accepted 22 November 2022; posted 23 November 2022 (Doc. ID 474387); published 30 January 2023

Nonlinear optics is a well-established field of research that traditionally relies on the interaction of light with macroscopic nonlinear media over distances significantly greater than the wavelength of light. However, the recently emerged field of optical metasurfaces provides a novel platform for studying nonlinear phenomena in planar geometries. Nonlinear optical metasurfaces introduce new functionalities to the field of nonlinear optics extending them beyond perturbative regimes of harmonic generation and parametric frequency conversion, being driven by mode-matching, resonances, and relaxed phase-matching conditions. Here we review the very recent advances in the rapidly developing field of nonlinear metasurface photonics, emphasizing multi-frequency and cascading effects, asymmetric and chiral frequency conversion, nonperturbative nonlinear regimes, and nonlinear quantum photonics, empowered by the physics of Mie resonances and optical bound states in the continuum.

https://doi.org/10.1364/PRJ.474387

1. INTRODUCTION

Optical metasurfaces have emerged recently as a very attractive planar technology for the realization of ultrathin optical elements with flexible and tunable control of light at the subwavelength level. Metasurfaces have come a long way in the last few decades, first as a two-dimensional realization of metamaterials [1,2] and then expanding rapidly in both design and applications far beyond the initial demonstrations, showing many fascinating phenomena with nanostructured surfaces and facilitating unique functionalities for a variety of practical applications [3,4]. Importantly, the fabrication capabilities and theoretical understanding have matured during that period to provide a solid background for the exploration of new concepts with metasurfaces [5]. Current efforts of many groups are focused on the study of tunable and active metasurfaces, including flexible control of structured light [6], which are expected to boost a range of metasurface applications in sensing technologies and light detection and ranging (LIDAR), augmented reality and dynamic holography, as well as many other applications discussed in this special issue.

Within this broad spectrum of novel opportunities, nonlinear metasurfaces emerged a few years ago as an exciting and potentially useful discipline [7]. Nonlinear metasurfaces allow wavelength conversion and switching that can be employed in optical information processing for planar switching and routing elements [8]. Initially, the nonlinear optics in metasurfaces was realized through plasmonic effects associated with metallic surfaces [9,10], for example, in the form of aperture arrays. The use of plasmonic metasurfaces was natural at that time because metallic elements allow us to achieve extreme subwavelength confinement, and they may support strong nonlinear optical response [9]. However, the downsides of using plasmonic metasurfaces are high dissipative losses and thermal heating that limit their applicability in nonlinear metaphotonics.

All-dielectric metasurfaces that support strong resonances of their meta-atoms provide a promising alternative to nonlinear plasmonics [11,12]. Metasurfaces made from high-index dielectric materials may support optically induced magnetic resonances that can enhance nonlinear effects together with electric nonlinearities usually employed in nonlinear optics [13]. Furthermore, low losses and high damage thresholds provide additional advantages for operating resonant metasurfaces at high pump intensities, thus allowing the enhancement of nonlinear processes moving to the regime of nonperturbative nonlinearities and high-harmonic generation.

Resonances play a crucial role in the physics of metasurfaces because they allow localization of light below the free-space diffraction limit by employing high-index dielectric nanostructures. First, Mie resonances are associated traditionally with the exact Mie solutions of Maxwell's equations for spherical particles [14]. In a broader context, they can be employed to control the enhancement of both electric and magnetic fields, being an important requirement for many nonlinear functionalities. In addition, bound states in the continuum (BICs) [15], being localized states of light residing in the radiation continuum, can provide an essential physical mechanism for trapping electromagnetic energy in open resonators for a substantial amount of time.

Thus, one can identify several physical mechanisms for electromagnetic field enhancement and mode engineering in resonant metasurfaces. This includes local resonances, such as surface plasmon resonances and Mie resonances of individual nanoparticles, as well as collective resonances, such as guided-mode resonances and BICs.

One critical issue of dielectric metaphotonics and metasurfaces is a relatively low refractive index at the visible and near-infrared (near-IR) frequencies. Increasing the refractive index by a modest factor using novel methods of material growth, fabrication, and subwavelength patterning will greatly impact imaging, integrated photonics, and other applications including nonlinear optics [16].

Metasurfaces can be fabricated with multiple degrees of freedom. They can combine various hybrid or composite materials such as graphene and two-dimensional single-layer semiconductors, promising novel opportunities for the exploration of nonlinear effects, generating nonlinear responses far beyond those of natural materials. The ability to design single "meta-atoms" and their arrays at will opens the way towards efficient engineering of the spatial nonlinear phase of the metasurfaces for the study of spin-controlled nonlinear interactions, directional nonlinear scattering, and nonreciprocal and topological effects.

Below, we discuss recent demonstrations of novel regimes and functionalities of nonlinear metasurfaces, as well as other applications of metasurfaces to nonlinear optics and photonics. In particular, we review the recent advances in the rapidly developing field of nonlinear metaphotonics emphasizing multi-frequency and cascading effects, nonlinear asymmetric imaging, chiral frequency conversion, nonperturbative nonlinear regimes, and nonlinear quantum photonics underpinned by the physics of Mie resonances and BICs.

2. FREQUENCY GENERATION AND WAVE MIXING

The optical response of the material to an external optical field, i.e., polarization $\mathbf{P}$, in dipole approximation can be expressed as power series that depends on the optical field strength $\mathbf{E}$,

$$\mathbf{P} = \varepsilon_0[\chi^{(1)}\mathbf{E} + \chi^{(2)}:\mathbf{EE} + \chi^{(3)}:\mathbf{EEE} + \ldots], \quad (1)$$

where ε_0 is the vacuum permittivity, and $\chi^{(n)}$ is the nth-order nonlinear susceptibility tensor. The second term of this equation describes second-order nonlinear processes such as second-harmonic generation (SHG) and sum frequency generation (SFG). The third term describes third-order nonlinear processes, including third-harmonic generation (THG) and four-wave mixing (FWM). These parametric nonlinear processes are phase sensitive; i.e., proper phase relationships between the pumping and newly generated waves should be maintained along the propagation direction of the light. In bulk nonlinear crystals, these interactions build up by propagating over tens to thousands of wavelengths; thus, phase-matching conditions can be fulfilled only for limited optical bandwidth. However, in metasurfaces, these interactions occur within nanoresonators of subwavelength dimensions that are typically much smaller than the coherence length, which relax phase-matching requirements and enable the simultaneous generation of multiple frequencies over a broad spectrum range [17,18].

Each component of the terms in Eq. (1) should be considered while designing a nonlinear metasurface: the value of nonlinear susceptibility, the spectral range of newly generated frequencies and transparency region of the material, the ability of the nanostructured design to enhance the local electromagnetic field through multipolar modes of Mie-type resonances, and the mode overlap between electromagnetic fields at the fundamental and newly generated frequencies. In the last couple of years, a wide variety of Mie resonances have been used to enhance light at the fundamental wavelength, including electric and magnetic dipole resonances [19–21], anapoles [22], and high quality factor (Q-factor) resonances [23–25], including BICs [26–30]. BICs provide exceptionally high electromagnetic field enhancement that drastically increases the field inside the nanoresonator by orders of magnitude, dramatically boosting the efficiencies of nonlinear processes. However, BICs often employ symmetry-broken resonator designs that require precise control over the design of the metasurface [31,32]. Quasi-BIC (q-BIC) resonances were demonstrated in silicon (Si) [28,29], aluminum gallium arsenide (AlGaAs) and gallium arsenide (GaAs) [26], gallium phosphide (GaP) [27,33], and, recently, hexagonal boron nitride (hBN) metasurfaces [34]. However, high-Q resonances in other material platforms employed for nonlinear metasurfaces including phase change materials, chalcogenide glasses, and various transitional metal dichalcogenides (TMDCs) are yet to be realized.

The high-Q-factor resonant mode at the fundamental wavelength is quite beneficial to boost the efficiency of the nonlinear process. But as implied in Eq. (1), field enhancement at the harmonic generation wavelength is favorable too. So far, the experimental realization of multiple high-Q resonances at all frequencies involved in the nonlinear process is quite challenging and has not been realized yet. Furthermore, while having highly resonant modes at all frequencies involved in the nonlinear process is desirable, it is not enough since the enhancement of nonlinear generation also depends on the spatial overlap of the electromagnetic field distributions with respect to the symmetry conditions imposed by the nonlinear tensor. The role of the electromagnetic field overlap is prominent between the two modes employed in frequency mixing processes such as SFG [35] and FWM [22,36] since it significantly affects the efficiency of the generated nonlinear process. However, for SHG and THG in metasurfaces, its role is diminished due to the high number of Mie modes excited at shorter wavelengths, which makes the field profile quite complex with a large variety of components.

This section briefly reviews nonlinear generation and frequency mixing in nonlinear metasurfaces. Tables 1 and 2 summarize recent developments in the field: materials that were used, nonlinear processes that were studied, linear and nonlinear properties, and if there is a study that reports high-Q resonance with Q-factors higher than 300. We highlight a few recent works utilizing new material platforms for harmonic

Table 1. Even-Order Nonlinear Processes in All-Dielectric Metasurfaces[a]

Material	Nonlinear Processes	Bandgap (eV)	$\chi^{(2)}$ (pm/V)	High-Q
GaAs	SHG [20,26,37], FHG [17][b], SFG [17,35], SWM [17][c]	1.42 [38]	$d_{14} \approx 209.5$ at 1058 nm [38]	Yes [26]
$Al_{0.18}Ga_{0.82}As$	SHG [39]	1.647 [40]	$\approx d_{GaAs} \cdot 0.9$ at 1064 nm [41]	Yes [26][d]
GaP	SHG [27,42], SFG [33]	2.26–2.78 [38]	$d_{36} \approx 70.6$ at 1064 nm [43]	Yes [27]
poly-$BaTiO_3$	SHG [44]	3.27–3.38 [45][e]	$d_{15} \approx 17$ at 1064 nm [38][e]	No
poly-ZnO	SHG [46]	3.5 [38][e]	$d_{33} \approx -5.86$ at 1058 nm [38][e]	No
$LiNbO_3$	SHG [47,48]	4 [38]	$d_{33} \approx -34$ at 1058 nm [38]	No
MoS_2	SHG [49,50]	1.29 [51]	$d_{surf} \approx 220$ at 900 nm [50][f]	No
hBN	SHG [34]	5.95 [52]	–	Yes [34]
a-Si	SHG [53,54]	1.7 [55]	–	Yes [56]
a-Se	SHG [57]	1.83–1.9 [58]	–	No

[a]In the table we present only the largest nonzero element of the $\chi^{(2)}$ tensor.
[b]Fourth-harmonic generation (FHG).
[c]Six wave mixing (SWM).
[d]Fabrication process is similar to GaAs metasurface.
[e]Crystalline material value.
[f]The value was measured for a monolayer.

Table 2. Odd-Order Nonlinear Processes in All-Dielectric Metasurfaces[a]

Material	Nonlinear Processes	Bandgap (eV)	$\chi^{(3)}$ (m^2/V^2)	High-Q
c-$Ge_2Sb_2Se_4Te_1$	THG [59]	0.3 [60]	3.36×10^{-18} at 4.5 μm [59][b]	No
a-$Ge_2Sb_2Se_4Te_1$	THG [59]	0.73 [61]	4.58×10^{-19} at 4.5 μm [59][b]	No
a-Ge	THG [62,63]	0.7 [64]	5.7×10^{-19} at 1650 nm [63][b]	No
c-Si/poly-Si	THG [28]	1.124 [38]	2.45×10^{-19} at 1550 nm [65]	Yes [28,66,67]
MoS_2	THG [49]	1.26 [51]	2.4×10^{-19} at 1560 nm [68]	No
GaAs	THG [17], FWM [17]	1.42 [38]	1.46×10^{-19} at 911 nm [69]	Yes [26]
a-Si/a-Si:H	THG [56,70,71]	1.7 [55]	6×10^{-19} at 1550 nm [12,72][b]	Yes [56,71]
As_2S_3	THG [73]	2.22–2.5 [38,74]	0.6×10^{-19} at 1550 nm [74]	No
TiO_2 rutile	THG [75]	3.5 [38]	5.6×10^{-20} at 1064 nm [76][b]	No

[a]Table 2 shows $\chi^{(3)}_{1111}$ or $\chi^{(3)}_{\mathrm{eff}}$ approximate values of third-order nonlinear susceptibilities.
[b]The value was measured for a thin film.

generation in the visible and ultraviolet (UV) ranges, review theoretical considerations about harmonic generation in metasurfaces, and show recent designs focused on the remaining constraints in conversion efficiencies of harmonic generation.

SHG is one of the most common effects studied in the field of nonlinear nanophotonics, specifically in nonlinear all-dielectric metasurfaces. SHG is a nonlinear process that requires a noncentrosymmetric structure of the material; thus, semiconductors, such as GaAs, AlGaAs, GaP, and lithium niobate ($LiNbO_3$) are commonly used. The first few recent works in the field of nonlinear metasurfaces and nanoresonators employed GaAs [20] and AlGaAs [77,78]. High nonlinear susceptibilities (see Table 1) of GaAs and AlGaAs are accompanied by significant absorption in the visible range of the spectrum that hinders newly generated nonlinear frequencies. A few recent works have begun to address this issue: there is a report about SHG [27] from a GaP metasurface with a wider bandgap of 2.26–2.78 [38] that holds the highest SHG efficiency in metasurfaces [12]. Another highly nonlinear material is $LiNbO_3$ [79]. The relatively large bandgap of $LiNbO_3$ ($E_{BG} = 4$ eV [38]) has permitted SHG in the visible range of the spectrum [47,48]; however, a $LiNbO_3$ metasurface with BIC resonance is yet to be realized, attributed partly to the difficulty of nanofabrication of $LiNbO_3$.

Since the SHG process strongly depends on the crystallographic structure of the material, the used GaAs [20], GaP [27], and $LiNbO_3$ [47] were monocrystalline. A few recent works explored SHG in metasurfaces fabricated from polycrystalline films, such as metal oxide barium titanate ($BaTiO_3$) [44] grown bottom-up by pulsed laser deposition and zinc oxide (ZnO) [46] sputtered on a soda lime glass substrate. Figure 1(a) shows polycrystalline $BaTiO_3$ nanoresonators composed of tightly packed nanoscale $BaTiO_3$ grains (20 nm to 200 nm) with a tetragonal crystal structure. The measured SHG efficiencies do not directly correspond to a specific second-order susceptibility $\chi^{(2)}$ tensor component but rather reflect an averaged $\chi^{(2)}$ that leads to an overall reduction of the SHG emission compared to a monocrystalline layer. Despite that, in both works the authors show a significant increase in SHG in the near-UV for the $BaTiO_3$ metasurface [44], and in the vacuum-UV spectrum range for the ZnO metasurface [46], in comparison with the unpatterned films due to the Mie-resonance enhancement. Moreover, in subsequent work on ZnO [80], Tseng *et al.* have successfully focused the vacuum-UV-band second harmonic in a self-emitting nonlinear ZnO metalens; see Fig. 1(b).

Discussed noncentrosymmetric materials support the generation of even and odd harmonics. However, surface nonlinearities

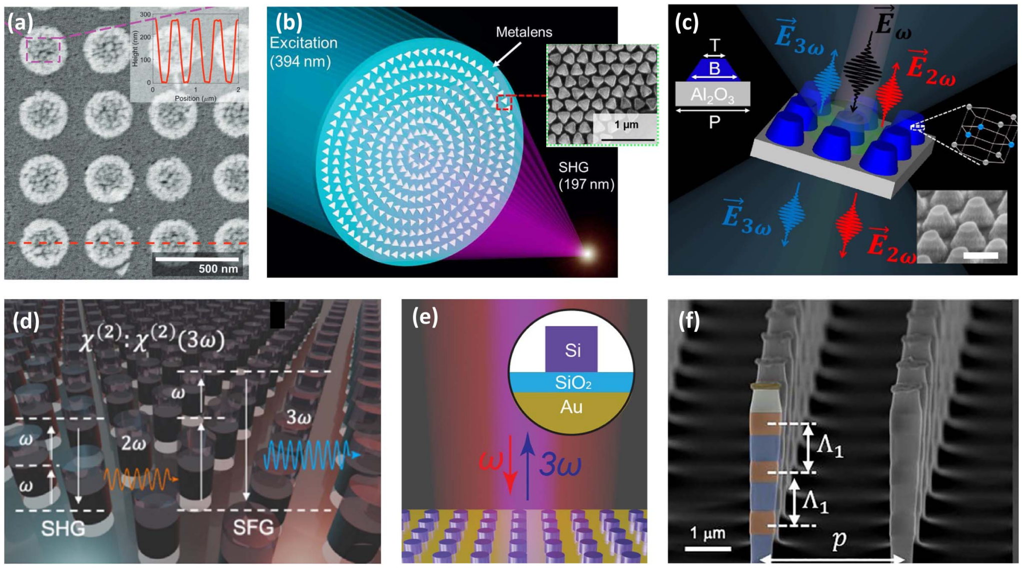

Fig. 1. Nonlinear resonant metasurfaces for second- and third-harmonic generation. (a) Scanning electron microscope (SEM) micrograph of $BaTiO_3$ nonlinear metasurface that operates in the near-UV spectral range. Inset: atomic force microscopy (AFM) height profile along the red dashed line [44]. Copyright Wiley-VCH Verlag GmbH & Co. KGaA. Reproduced with permission. (b) Schematic illustration of ZnO-based nonlinear metalens focusing self-generated vacuum-UV second harmonic. Inset: SEM image of the fabricated metalens. Adapted from Ref. [80]. Licensed under CC BY-NC 4.0. (c) Schematic of crystalline transition-metal-dichalcogenide truncated cone metasurface that enables single-beam second- and third-harmonic generation. The bottom-right inset shows the SEM image of the fabricated MoS_2 metasurface. Reprinted with permission from Macmillan Publishers Ltd. [49]. Copyright 2021. Licensed under CC BY. (d) Artistic representation of the dielectric metasurface with THG at frequency 3ω generated via cascaded SHG and sum-frequency generation process: $3\omega = \omega + 2\omega$. Reprinted with permission from Ref. [81]. Copyright 2022 American Chemical Society. (e) Design of Si metasurface on a gold mirror that enables BIC resonance for THG enhancement. The inset shows the cross section of the unit cell with corresponding materials. Reprinted with permission from Ref. [29]. Copyright 2022 American Chemical Society. (f) SEM image of a three-layer GaAs-based nonlinear metasurface for second-harmonic generation (SHG). Adapted from Ref. [82]. Licensed under CC BY 4.0.

can also play a significant role and boost SHG in centrosymmetric materials [49–58]. One intriguing group of materials is TMDCs such as molybdenum disulfide (MoS_2) and tungsten diselenide (WSe_2)—van der Waals materials with high refractive index and relatively large bandgap in the near-IR and visible range of the spectrum. Recent nonlinear studies show that exfoliated monolayers of TMDC exhibit extremely high nonlinear susceptibilities with $\chi^{(2)}$ that can range from 1.2 to 10^5 pm/V [83], with enhancement originating from the overlap of SHG wavelength with the C-exciton of TMDC [84,85]. This fact was taken advantage of in the paper by Popkova *et al.* [50], where the authors demonstrate a Mie-resonant metasurface from a thick flake of MoS_2 and show enhanced SHG that is generated at a wavelength that overlaps with the C-exciton. As a result, the MoS_2 metasurface produced a 23-fold enhancement of SHG intensity with respect to the exfoliated unpatterned monolayer of MoS_2. As mentioned earlier, since bulk 2H-MoS_2 has D6h point group symmetry and is centrosymmetric, the measured second-order nonlinear response likely comes only from the top and bottom surfaces of the nanoresonators.

A similar result was demonstrated in an earlier paper by Nauman *et al.* [49], where both SHG and THG are enhanced in a Mie-resonant metasurface that consists of an array of Mie-resonant truncated cones [Fig. 1(c)]. In this paper, the authors also show the benefits of the extremely high refractive index of MoS_2 by designing a metasurface that operates in a subdiffractive regime for nonlinear harmonics and therefore generates directional emission of SHG and THG.

The results shown are captivating and provide an excellent base to further explore TMDCs as a possible material platform for nonlinear metasurfaces. So far, only hBN-based metasurfaces that support BIC resonances were experimentally realized [34]. One of the reasons can be difficulty in fabrication process development since each sample is unique, and its optical properties depend on an exfoliated flake. The lateral size of the flake is typically a few tens of micrometers—such a small working area and uncertainty of exfoliated flake thickness complicate the process, increase the fabrication time, and limit the repeatability and desirable control of the nanostructure design.

Table 2 summarizes various materials that were employed for THG and FWM processes that rely on $\chi^{(3)}$ nonlinear susceptibility, including Si, Ge, TiO_2, phase change materials such as germanium antimony selenide telluride (GSST) [59] and germanium antimony telluride (GST) [86], and chalcogenide glasses, such as arsenic trisulfide (As_2S_3) [73]. Unlike with SHG, there are no restrictions in crystallographic symmetry, and any material can be utilized.

As we mentioned previously, not only material selection plays a role in nonlinear frequency conversion. In the following paragraph, we show a few recent works that provide insight into the nonlinear generation in metasurfaces and propose new designs to enhance the efficiencies of nonlinear harmonics.

From the previous example with MoS_2, we saw that metasurfaces could support the simultaneous generation of multiple nonlinear processes, such as SHG and THG, due to the relaxed phased matching conditions between fundamental and nonlinear frequencies [17,49]. However, there has been a debate about the nature of these processes: is it a pure frequency multiplication, or do cascaded nonlinearities play a role? One of the recent works [81] explores this question and analyzes SHG and THG processes in a GaAs metasurface in conjunction with polarization selection rules and crystal symmetries [Fig. 1(d)]. The authors demonstrate different contributions to the signal at the THG frequency and show that a significant part of it originates from the mixing fundamental wavelength with the surface second harmonic. This work experimentally confirms the importance of surface nonlinearities in nonlinear metasurfaces and shows that further analyses could provide additional control over nonlinear frequency mixing.

Interestingly, in a large number of works, nonlinear optical harmonics in metasurfaces are generated in the opaque region. In Ref. [73] the authors highlight this question and show that in metasurfaces the THG process can be enabled by a phase-locking mechanism between the pump and the inhomogeneous portion of the third-harmonic signal [87,88]. The propagation of this inhomogeneous THG component is not affected by the material dispersion and absorption at the THG wavelength, thus enabling efficient frequency conversion in the absorptive region. This theory is quite intriguing and is incredibly important for vacuum–UV light generation, where only a few nanometers of material are expected to contribute to harmonic generation. We hope to see further experiments that can provide additional insight to this theory.

As previously stated, electromagnetic field enhancement is an important aspect of harmonic generation. A great deal of previous research in nonlinear Mie-resonant metasurfaces discusses and employs high-Q-factor photonic modes such as q-BICs that can significantly increase the efficiencies of newly generated nonlinear frequencies. The record-breaking efficiencies of nonlinear harmonics achieved in metasurfaces [27,28] utilize BICs that rely on symmetry breaking, either by using asymmetric geometries of nanoresonators [89] or by using a non-normal incident angle. One of the recent works [29] demonstrates that BICs can be achieved in metasurfaces by using magnetic dipole resonances coupled to a mirror. The introduced design does not require broken symmetry or depend on incident polarization: it is an array of silicon nanodisks that sits on top of a thin dielectric layer with a mirror underneath [Fig. 1(e)]. To show the performance of the metasurface, the authors demonstrate THG that benefits from the strongly enhanced electric field at BIC resonance. Measured THG efficiencies are the highest reported so far using femtosecond laser pulses, $P_{\mathrm{THG}}/P_{\mathrm{pump}} = 1.8 \times 10^{-6}$.

As the Q-factors in metasurfaces break records, the bandwidth mismatch between the laser pulse and the resonance decreases the possible harmonic efficiency. The emerging field of high-Q time-variant metasurfaces, where the refractive index of the metasurface rapidly varies at the timescale of a pump pulse duration, shows how to overcome that by introducing a chirp to the pump pulse [90]. Another way to match the bandwidth with the resonance is by pumping the high-Q metasurface with a continuous wave laser. With other requirements for efficient harmonic generation fulfilled, such as a high nonlinear coefficient, BIC-boosted enhancement at the fundamental wavelength, and newly generated wavelength in the material's transparency region, the highest to date efficiency of the nonlinear generation process was achieved in the GaP metasurface [27], $P_{\mathrm{SHG}}/P_{\mathrm{pump}} = 4 \times 10^{-5}$. The normalized conversion efficiency [12] is $(P_{\mathrm{SHG}}/P^2_{\mathrm{pump}}) \cdot d = 8 \times 10^{-4}\ \mathrm{W}^{-1}$, where P_{SHG} is the SHG peak power, P_{pump} is the peak power of the incident pump, and d is the spot size divided by the unit cell size.

A different direction to boost nonlinear frequency conversion has been considered in a few other recent studies: to enhance generated harmonics, authors use multilayered metasurfaces [82,91]. For example, Marino *et al.* [82] demonstrate a GaAs metasurface that consists of three layers of nanodisks [Fig. 1(f)]. When the metasurface is pumped at its magnetic dipole resonance, the use of a few layers improves the SHG efficiency by 15 times with respect to its one-layer counterpart. Despite increased complexity in the fabrication of multilayered nanostructures, we believe that it is a feasible direction in nonlinear metaoptics since it increases the interaction length of the fundamental pump with the material that can enhance the nonlinear generation and provide an additional degree of freedom to control nonlinear generation.

In this section, we have provided an overview of the recent advances in SHG and THG in nonlinear metasurfaces to show the possible pathways for further studies in this area. Developing new fabrication techniques and exploring new materials is essential and can provide us with novel functionalities of nonlinear metasurfaces. For example, harmonic generation in electro-optic materials such as $BaTiO_3$ and $LiNbO_3$ can show electrical control [92,93] and tunability of nonlinear response [79]; chalcogenide glasses, such as As_2S_3, are also quite promising for nonlinear frequency all-optical control, which has been reported just recently [94]. Moreover, merging different materials, including metasurfaces with TMDC flakes [95–99], also shows new pathways for nonlinear frequency conversion. Finally, further development of the fabrication process of multilayered metasurfaces [82,100,101] will allow us to control the optical nonlinear response of each layer separately, which will definitely be beneficial in nonlinear metadevices.

3. NONLINEAR IMAGING AND ASYMMETRIC PARAMETRIC GENERATION

One of the important directions of the recent research is the demonstration of nonlinear holographic metasurfaces composed of dielectric resonators such as C-shaped Si nanoantennas [66]. In this case, the incident laser is enhanced by their fundamental resonance, whereas the generated third-harmonic signals create high-efficiency nonlinear holograms. On the other hand, nonlinear metasurfaces can facilitate new phenomena including the imaging of objects through a dielectric nonlinear metalens [102]. Schlickriede *et al.* [102] illuminated objects by infrared light and recorded their generated images at the visible third-harmonic wavelengths. The authors suggested a generalized Gaussian lens equation for nonlinear imaging, verified both experimentally and analytically.

As a characteristic example of the most recent achievements in the field of nonlinear resonant metasurfaces, below we discuss the recent demonstration of asymmetric parametric generation of light with nonlinear bianisotropic metasurfaces reported by Kruk *et al.* [103], where third-harmonic images are generated for two reversed directions of illumination when the positions of the infrared emitter and the visible light receiver are exchanged.

We notice that one of the important proposed functionalities of metasurfaces is associated with asymmetry in both the generation and transmission of light with respect to reversals of the positions of emitters and receivers. Nonreciprocity arises in various branches of physics, where it underpins many phenomena and applications [104]. A nonreciprocal system is defined as a system that exhibits different received–transmitted field ratios when its source and detector are exchanged. In electromagnetism, nonreciprocity was first experimented by Faraday in 1845, explicitly described by Stokes in 1840 and by Helmholtz in 1856, reformulated by Kirchhoff in 1860, anticipated in nonlinear media by Rayleigh in 1873, and extensively applied by Planck in 1900 in connection with blackbody radiation [104].

Nonreciprocity may be generally classified as either linear or nonlinear. In both of those cases, it results from breaking time-reversal symmetry, by an external bias force in the linear case, and by a combination of self-biasing and structural asymmetry in the nonlinear case [104]. In the nonlinear case, nonreciprocity can be realized with nonlinear light–matter interaction in metasurfaces as was suggested theoretically a few years ago [105,106]. Mahmoud [105] suggested to create a Faraday rotator without an external magnetic field, by employing chiral metasurfaces combined with nonlinear elements integrated into a Fabry–Perot cavity. For nonlinear response, the authors suggested to employ varactor diodes with the realization for microwaves.

Bianisotropy was suggested for achieving asymmetric optical response, including asymmetric reflection, absorption, optical forces, light trapping, and lasing. These asymmetric effects originate from magnetoelectric coupling and asymmetrical field enhancement. In the linear regime, breaking symmetry of all-dielectric nanoparticles led to geometrically tunable magnetoelectric coupling and different backscattering scenarios [107]. These theoretical predictions were verified in experiment [108] for bianisotropic particles supporting both electric and magnetic Mie-type resonances, revealing that the particle with broken symmetry exhibits different backscattering for the opposite excitation directions. A metasurface composed of such bianisotropic particles demonstrates that the metasurface is characterized by different reflection phases when being excited from the opposite directions [108].

Mobini *et al.* [109] suggested theoretically to employ this scattering asymmetry for highly asymmetric SHG in bianisotropic AlGaAs metasurfaces. The authors demonstrated that the theoretical ratio of second-harmonic power for the forward and backward illuminations can be increased by around four orders of magnitude. This effect is obtained by altering geometrical parameters that coincide with q-BIC resonances. They argued that this directional generation of higher-order waves can be potentially useful for nonlinear holograms.

The first experimental demonstration of asymmetric third-harmonic nonlinear metasurfaces was reported recently by Kruk *et al.* [103]. The authors suggested theoretically and demonstrated in experiment all-dielectric metasurfaces producing a nonlinear asymmetric generation of light. When infrared light passes through the metasurfaces, specifically encoded images

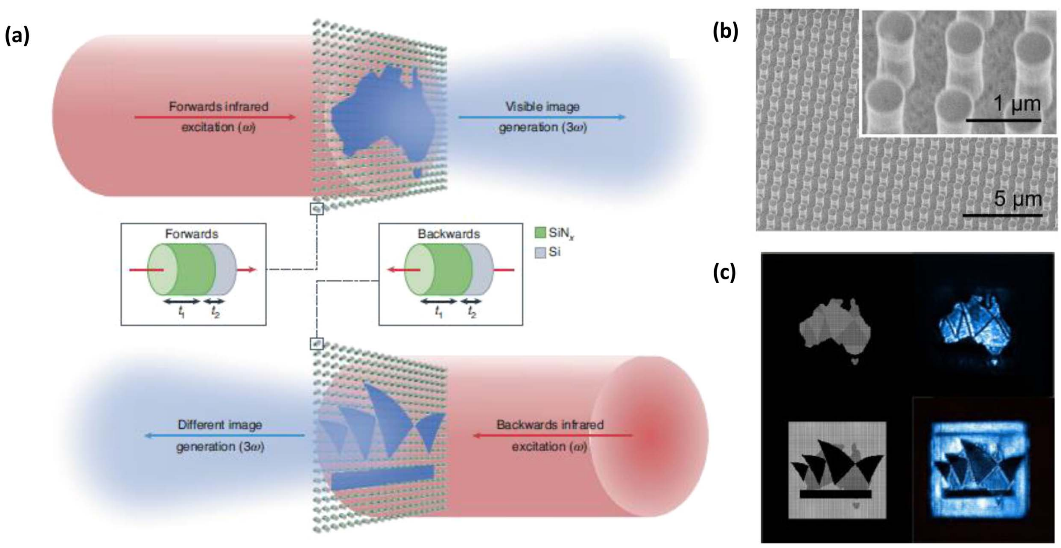

Fig. 2. Asymmetric generation of third-harmonic images with nonlinear nonreciprocal metasurfaces. (a) Directional formation of images achieved at the third-harmonic-generation frequency by using nonlinear anisotropic dielectric metasurfaces with asymmetric geometry and strong magneto-optical coupling [110]. The unit cell is composed of subwavelength nanoresonators based on silicon nitride and amorphous silicon. (b) Experimental realization of the bilayer metasurface: scanning electron microscopy image of the sample, before its embedding into the homogeneous environment. (c) Experimental results. Nonlinear optical response detected in transmission at the third-harmonic frequency for forward and backward excitation at a wavelength of 1475 nm. Each experimental image is assigned its own individual minimum and maximum levels of camera counts. Adapted from Ref. [103]. Copyright 2022 Springer Nature Ltd.

are observed, as presented in Fig. 2. But when the authors flipped the metasurfaces to the opposite side, they observed completely different images.

Figure 2(a) presents the main concept of asymmetric generation of the third-harmonic images with metasurfaces when the harmonic fields are generated differently in both forward and backward directions of excitation. Such nonlinear metasurfaces have been realized in experiment by creating lattices of bilayer bianisotropic resonators as shown in Fig. 2(b) embedded into a homogeneous environment. With these bianisotropic metasurfaces, the third harmonic is generated asymmetrically for two different propagation directions. The experimental results are presented in Fig. 2(c), which shows the nonlinear images detected for the third-harmonic fields in transmission for forward and backward excitation at a wavelength of 1475 nm [103].

Finally, we mention other recent theoretical proposals [111,112] for creating nonreciprocal nonlinear metasurfaces in the absence of any external bias to obtain free-space nonreciprocity. This is achieved by introducing a nonlinear Kerr-like response demonstrating that for certain input intensities the metasurface can become highly nonreciprocal, allowing large transmission in one direction and low transmission in the other. The first experimental demonstration of such nonlinearity-induced nonreciprocity in free-space metasurfaces has been reported just recently by Cotrufo *et al.* [113] who implemented this concept for free-space radiation using silicon metasurfaces supporting asymmetric q-BIC resonances.

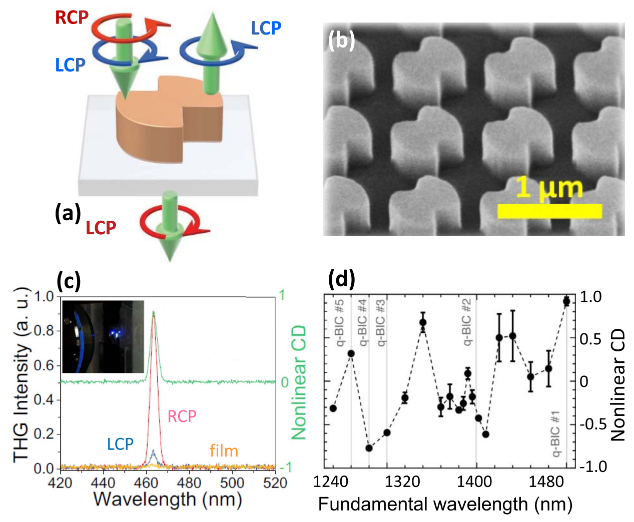

Fig. 3. Examples of enhanced nonlinear chiral response of metasurfaces. (a), (b) Optical chiral quasi-BIC metasurface composed of arrays of meta-atoms resonantly transmitting RCP light but transforming it to LCP light. (c) Experimentally measured THG intensities for chiral metasurface, compared to Si thin film. Inset shows a photographic image of the light spot of THG. Adapted from Ref. [116]. Licensed under CC BY 4.0. (d) Measured third-harmonic chiral dicroism spectrum in nonlinear dielectric metasurface that supports multiple quasi-BIC resonances. Dashed lines are guide for eyes. The resonant wavelengths are marked with solid vertical lines [118].

4. NONLINEAR CHIRAL METASURFACES

Many phenomena in nature, including multiple biochemical processes, are governed by the fundamental property of chirality. An object is called chiral when its mirror image cannot be superimposed with the original object, and many examples of chirality can be found at all scales in nature, from organisms to biomolecules and amino acids, which often occur only in one handedness. Circular dichroism (CD) spectroscopy was suggested as a powerful optical technique for the study of chiral materials and molecules. It gives access to an enantioselective signal based on the differential absorption of right and left circularly polarized light. In natural media, chiral effects are weak, so that chiral plasmonic structures and chiral metamaterials were suggested as a new tool for achieving strong chiroptical responses [114].

Here we discuss how to enhance linear and nonlinear circular dichroism in dielectric metasurfaces with optically induced Mie resonances [14] and chiral BICs [115].

Shi *et al.* [116] employed the symmetry-reduced dielectric metasurfaces composed of "meta-atoms" with high birefringence supporting winding elliptical eigenstate polarizations with opposite helicity. Figures 3(a) and 3(b) show an example of a chiral metasurface supporting chiral BIC resonances. Shi *et al.* [116] demonstrated experimentally chiroptical responses with ultrahigh Q-factors (up to $Q \approx 600$) and near-perfect circular dichroism ($\mathrm{CD} \approx 0.93$) at optical frequencies.

Circularly polarized light interacting with resonances of nanostructures in the nonlinear regime and nonlinear chiral metasurfaces has been studied intensively for plasmonic structures and plasmonic metasurfaces where the nonlinear signal originates from "hot spots" being dependent on the handedness of the nanostructures [117]. Dielectric chiral BIC metasurfaces can realize maximal nonlinear CD with promising active chiral applications.

Figure 3(c) shows the experimentally measured THG intensity under RCP/LCP pumping. Clear THG emission contrast yields nonlinear CD as high as 0.81. The THG efficiency is significantly enhanced by the q-BIC resonances, as compared to the THG emission intensity by a reference Si thin film. Limited by the operating band and loss of the objective lens, the effect of THG visible to the naked eye can be realized when the incident power is large enough, as shown in the inset of Fig. 3(c) [116].

The resonant metasurfaces supporting chiral BICs may provide a route to the study of chiral light–matter interaction for many types of photonic systems based on quantum dots and halide perovskites or operating with small chiral molecules. This approach allows the experimental realization of inherent chirality with BIC-resonant dielectric metasurfaces that may improve the design of chiral sources of light and boost the applications of chiral metasurfaces in photonic and quantum systems.

Very recently, Koshelev *et al.* [118] engineered a chiral silicon metasurface with L-shaped meta-atoms for enhanced nonlinear chiroptical response of THG, as shown in Fig. 3(d). They demonstrated theoretically and observed in experiment the pronounced circular dichroism (CD) at the Mie and q-BIC resonances. The transmission spectra for LCP and RCP pumps demonstrate the increase of linear chirality in the vicinity of the resonances [118]. In addition, strong nonlinear chiroptical response associated with high efficiency of the THG leads to large nonlinear circular dichroism varying from $+0.918 \pm 0.049$ to -0.771 ± 0.004 for the samples with different asymmetries. We notice that the reported value of nonlinear circular dichroism exceeding 0.9 is record high compared to the CD values for nonlinear metasurfaces reported earlier.

Finally, we mention that Frizyuk *et al.* [119] studied the nonlinear response of a dimer composed of two identical Mie-resonant dielectric nanoparticles illuminated normally by a circularly polarized light. They have developed a general theory describing hybridization of multipolar modes of the coupled nanoparticles and revealed nonvanishing nonlinear circular dichroism in the SHG signal enhanced by the multipolar resonances in the dimer, provided its axis is oriented under an angle to the crystalline lattice of the dielectric material.

5. STRONG NONLINEAR EFFECTS

When light interacts with materials, weak nonlinear effects are manifested in the generation of the lower harmonics, including the second or third harmonics, and they can be described by a conventional perturbation theory. However, sufficiently intense light can temporarily modify optical properties of the material proportional to the amplitude of the incident light. Such strong light–matter interaction regimes can lead to novel phenomena, such as an induced shift of the frequency of the generated harmonics, multiphoton absorption, as well as the generation of higher harmonics with relatively strong intensities. Recent progress in the physics of resonances supported by dielectric metasurfaces allows experimental observation of such effects, due to the energy concentrations on scales smaller than the wavelength of light. As discussed in the recent review paper [120], engineered optical resonances play an important role in the field of nanoscale nonlinear optics, and they can intensify electromagnetic fields within nonlinear materials by orders of magnitude. Below, we describe several of such effects facilitated by strong light–matter interaction in resonant metasurfaces.

As described above, dielectric metasurfaces can support sharp optical resonances enabled by the BIC physics observed in experiments as q-BIC resonances with large but finite Q-factors. The BIC resonances allow the enhancement of light–matter interaction at the subwavelength scale facilitating strong nonlinear effects. Strong narrow-band field enhancement in q-BIC metasurfaces leads to a change of the refractive index not described by perturbative theories. Sinev *et al.* [121] demonstrated such effects in the study of ultrafast self-action effects in silicon metasurfaces revealed in the nonlinearity-induced dependence of the THG efficiency. They observed experimentally a transition from the subcubic to super-cubic regimes for the generated third-harmonic light in the multiphoton absorption regime.

Figures 4(a) and 4(b) summarize the observation of self-action effects with resonant silicon metasurfaces [121]. The authors employed a silicon metasurface with an asymmetric unit cell composed of two parallel bars of different widths [see the inset to Fig. 4(b)] supporting a spectrally sharp transmission resonance in the near-IR with a Q-factor of about 900. The observed blue shift of the TH wavelength above the threshold value of the pump power can be associated with the self-action effects of subpicosecond laser pulses, as illustrated in Fig. 4(a), driven by a strong field ionization in nanostructured silicon induced by multiphoton absorption [121]. Figure 4(b) shows the experimentally measured dependence of THG spectra on pump power; each spectrum is normalized to the third power of its pump intensity.

To evaluate the optical response of silicon metasurface, Sinev *et al.* [121] used the theory employing Keldysh photoionization

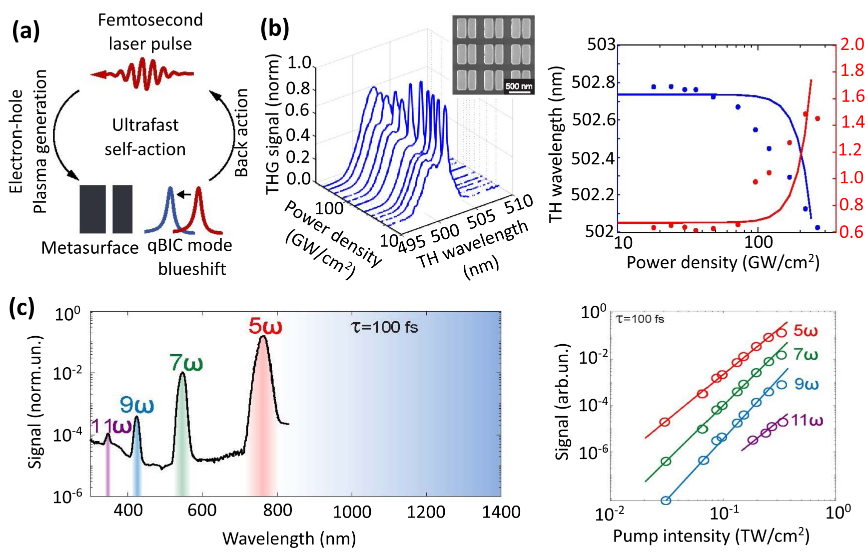

Fig. 4. Observation of self-action effects and high-harmonic generation with resonant silicon metasurfaces. (a) Scheme of the ultrafast self-action effects in the metasurface supporting quasi-BIC resonances. (b) Experimentally measured dependence of THG spectra on pump power; each spectrum is normalized to the third power of its pump intensity. Right: measured (dots) and simulated (solid lines) evolution of the spectral position (blue) of the THG peak and its linewidth (red) with an increase of the pump power density. Inset shows an SEM image of the resonant metasurface. Adapted with permission from Ref. [121]. Copyright 2021 American Chemical Society. (c) Spectrum of high harmonics generated by 100 fs laser pulses. The pale blue area is the spectral range not covered for a particular spectrometer. Right: power dependence of the generated fifth to eleventh harmonics for 100 fs pump pulses. Adapted with permission from Ref. [122]. Copyright 2022 American Chemical Society.

with a direct bandgap for silicon as the main source for the conduction band carrier density. Within this approach, the refractive index changes can be derived from the Drude-like model with the modified laser-induced electron plasma. Then, the homogeneous distribution of free carriers inside silicon nanostructures is assumed. The authors compared the pump-dependent change of the wavelength of the generated third harmonics, and its linewidth shown in Fig. 4(b). In the experiment, the peak blue shifts by 0.6 nm with the change of pump power from 20 to 200 GW/cm^2. The measured mode linewidth increases to two and a half times with a growth of the pump power. This numerical model predicts a similar change of the linewidth and peak position shown with solid lines in Fig. 4(b). The numerical model predicts a growth of the concentration of free carriers up to values of 5×10^{18} cm^{-3} for pump power densities corresponding to the power of 10 mW.

The concept of optical BICs can be employed to generate high harmonics from dielectric metasurfaces and observe experimentally the transition from perturbative to nonperturbative regimes of nonlinear optics. Zograf *et al.* [122] designed silicon metasurfaces supporting q-BIC resonances in the mid-IR frequency range. The BIC resonance at the fundamental wave allows strong energy concentration in the metasurfaces boosting the generation of higher harmonics, namely from third to eleventh odd optical harmonics extending through the near-IR to the visible spectral ranges, as shown in Fig. 4(c). They confirmed that the observed harmonic generation originates from the power enhancement realized for the optimal metasurface geometry, and they have studied the dependence of the fifth harmonic on the pump, with a deviation from the perturbative regime. Zograf *et al.* [122] observed a dramatic efficiency enhancement and spectral narrowing of the high-harmonic generation for varying the pump pulse duration from the subpicosecond to the picosecond regime.

Another observation of high-harmonic generation from metasurfaces was reported by Shcherbakov *et al.* [123] who demonstrated highly efficient high-harmonic generation from GaP metasurfaces driven by intense mid-IR laser pulses. They observed the generation of even and odd harmonics covering a wide range of photon energies between 1.3 eV and 3 eV with minimal reabsorption. The resonantly enhanced conversion efficiency facilitates single-shot measurements that avoid material damage and pave the way to study the controllable transition between perturbative and nonperturbative regimes of light–matter interactions at the nanoscale.

High-order harmonic spectra strongly depend on the crystal orientation with respect to the driving laser polarization. Notably, even-order harmonics would coexist with odd-order harmonics only if the intrinsic inversion symmetry of the material is broken [124–126]. The mechanisms responsible for the generation of nonperturbative odd and even high-order harmonics are currently under debate and attributed to different quantum phenomena in semiconductors, such as intraband and interband transitions [127], quantum interference and interplay of direct (from valence to conduction band) and indirect (involving multiple bands) transitions [128], but also transition dipole amplitude and phases [125] and a finite Berry phase [129]. These effects can be explored theoretically by first-principles studies using time-dependent density functional theory (TDDFT) or by solving semiconductor Bloch equations (SBEs) for a particular electronic multiband structure [130]. The latter quantum approach is less computationally expensive and can be coupled to Maxwell equations to investigate the nonlinear optical response of single resonators or even metasurfaces [131].

One of the future strategies to tailor nonlinear effects such as high-harmonic generation and nonlinear frequency mixing is to explore multiple resonances in metasurfaces. In particular, Xiao *et al.* [132] (see also Ref. [133]) suggested theoretically a novel approach for dynamically switchable high-harmonic generation metasurfaces by exploiting polarization-controlled dual BIC resonances. They calculated numerically efficient third- and fifth-harmonic generation from direct parametric processes and cascaded processes based on degenerate FWM. They demonstrated that the BIC resonances and generated harmonics enhanced resonantly by BICs can be switched on or off with high selectivity with respect to the fundamental pump polarization. This approach provides an effective tuning mechanism exploring the polarization degree of freedom for switchable nonlinear subwavelength sources of light.

Another interesting approach to expand the bandwidth of the resonant interactions in resonant metasurfaces is based on the concept of Q-boosting, where the Q-factor of a metasurface rapidly increases with time. Shafirin *et al.* [134] employed coupled-mode theory to demonstrate that the bandwidth limit of dielectric silicon–germanium metasurfaces can be expanded by coupling a broadband signal to a bandwidth-matched resonance realizing Q-boosting at a timescale faster than a resonator lifetime. They predicted the third-harmonic enhancement by factors of 8 (peak) and 4.5 (integrated) against the best-case static metasurface.

6. QUANTUM NONLINEAR OPTICS

Rapid progress in quantum technologies has not left aside the field of all-dielectric metasurfaces [135]. Flat optical metasurfaces have a future to become essential building blocks for on-chip quantum light sources, optical components, routing elements, as well as single-photon detectors that are vital in various applications, including quantum computing, quantum information, quantum sensing, and quantum communication [136].

Below we review very briefly recent progress in nonlinear metasurfaces as nonclassical light sources. Specifically, we discuss the recent studies of photon-pair generation in dielectric metasurfaces through the simplest nonlinear optical processes, being spontaneous parametric downconversion (SPDC), first observed in Ref. [137]. In SPDC, a pump photon splits into two daughter photons, called signal and idler. The emission of such a pair can be viewed similarly to the spontaneous emission of single photons: the pump photon excites the nonlinear system and then the two-photon spontaneous transition down brings the system back to the ground state. This transition, mediated by the second-order susceptibility, leads to the spontaneous emission of a photon pair. Like a single-photon transition, it requires the vacuum field for its explanation. Similarly, the enhancement of this vacuum field due to a resonance at one

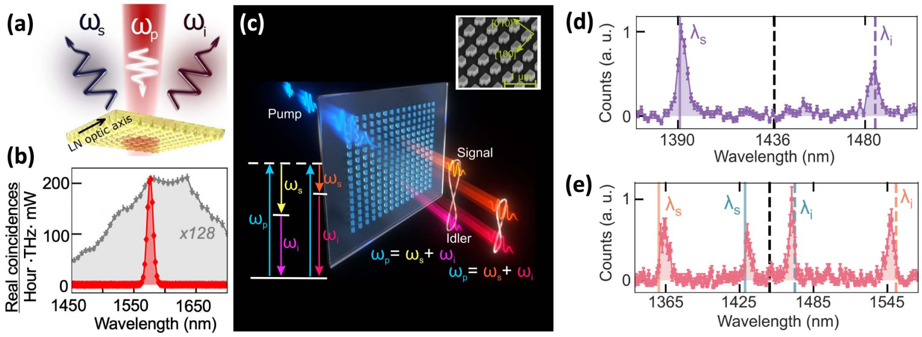

Fig. 5. (a) Artist's representation of SPDC from a $LiNbO_3$ metasurface: the pump ω_P is incident from the substrate side; photon pairs ω_s and ω_i are collected in reflection. (b) Spectrum of production of photon pairs enhanced by Mie resonance in $LiNbO_3$ metasurface shown by red diamonds, referenced to unpatterned film of the same thickness shown by gray stars. Reprinted with permission from Ref. [141]. Copyright 2021 American Chemical Society. (c) Schematic illustration of multiplexed entangled photon generation in a multi-resonance semiconductor metasurface. Inset shows SEM image of GaAs metasurface that supports BIC resonance before metasurface was transferred on the transparent substrate. (d) Measured SPDC spectra of non-degenerate photon pairs in GaAs metasurface where the signal photon is emitted at the electric dipole BIC mode wavelength (purple vertical solid line). (e) Measured SPDC spectra of GaAs metasurface when two types of non-degenerate photon pairs are produced: signal photons are emitted at wavelengths of electric dipole BIC resonance (orange solid vertical line) and the magnetic dipole BIC resonance (green vertical solid line) [142].

of the frequencies increases the probability of a two-photon transition.

As we would expect from the quantum-classical correspondence principle, nonlinear Mie-type optical nanoresonators and metasurfaces that are made from highly nonlinear materials, relax phase-matching conditions (i.e., momentum conservation), and have resonant enhancement of electromagnetic fields can also be used to enhance vacuum fluctuations by orders of magnitude. This was recently predicted theoretically [138,139] and realized experimentally using single nanoresonators [140], Mie-resonant metasurfaces [141,142], and metasurfaces with nonlocal resonances [143]. The first demonstration of Mie-resonant photon-pair generation via SPDC in all-dielectric metasurfaces used an array of truncated pyramids made from $LiNbO_3$; see Fig. 5(a) [141]. The authors showed two orders of magnitude enhancement of degenerate photon-pair production in the metasurface in the vicinity of the Mie resonance with a Q-factor of 100, compared with an unpatterned film of $LiNbO_3$ of the same thickness [Fig. 5(b)]. An order of magnitude higher rate enhancement of photon-pair generation was achieved in later works that use high-Q resonances such as nonlocal resonances in silica-glass metagratings fabricated on top of $LiNbO_3$ thin film [143], and Mie-type q-BIC resonances in broken-symmetry GaAs metasurfaces [142]; see Fig. 5(c).

More interestingly, when the pump wavelength is not precisely at half of the frequency of the resonance, the metasurface emits one photon of the pair ω_s at the resonance wavelength, and the conjugate photon ω_i at the wavelength defined by the energy conservation law $\omega_p = \omega_s + \omega_i$. Such non-degenerate biphotons were demonstrated recently in the previously mentioned GaAs metasurface [142]: SPDC spectra [Fig. 5(d)] exhibit two peaks at the wavelengths of the signal λ_s and idler λ_i photons, and only the signal photon wavelength overlaps with the BIC resonance wavelength. In that case, the idler photon wavelength can be spectrally tuned by changing the pumping wavelength without losing the rate of SPDC. Because the vacuum field seeds SPDC uniformly over the spectrum, and because momentum conservation is relaxed, multiple efficient SPDC processes can be driven simultaneously in a multi-resonant metasurface. Two pairs of non-degenerate entangled photons in SPDC spectra were measured for the metasurface that supports two Mie high-Q resonances at λ_s wavelengths; see Fig. 5(e).

The authors in Refs. [142,143] also show the violation of the Cauchy–Schwartz inequality to prove the generated photons' nonclassical nature and entanglement state. Furthermore, nonlinear metasurfaces with high-Q resonances and relaxed momentum conservation create a way to generate cluster quantum states [142]—entangled states of multiple photons when multiple pumping sources are used. These cluster states are building blocks in one-way quantum computation and are impossible to be produced in bulk nonlinear crystals.

Li *et al.* [144] took a different approach: the authors integrated an array of 10 × 10 gallium nitride metalenses with nonlinear beta-barium borate (BBO) crystal and demonstrated a 100-path SPDC photon-pair source. Two-, three-, and four-dimensional two-photon path entanglement was experimentally confirmed. Moreover, multiphoton state generation was also shown. The purity and indistinguishability of four- and six-photons produced by different metalenses were confirmed using Hong–Ou–Mandel interference. The metalens-array-based quantum photon source provides a route for the generation and control of complex quantum states and is promising for the development of compact integrated quantum devices.

The field of nonlinear quantum metasurfaces is on the rise, and, similar to classic nonlinear metasurfaces, we expect it to broaden to other materials, designs, and functionalities (see Refs. [145,146]). For example, SPDC in thin films of GaP was reported just recently [147]. We believe that in future works, nonlinear quantum metasurfaces will be used for nonclassical light generation via SPDC and spontaneous four-wave mixing (SFWM) in a broad range of the spectrum, from UV to IR, with unique tunable properties of generated quantum states, such as entanglement, polarization, direction, orbital angular momentum, and wavelength.

7. CONCLUSION AND OUTLOOK

Nonlinear optics requires efficient methods for nonlinear properties engineering. In bulk media, this engineering is achieved by selecting appropriate crystals with anisotropic properties or by employing the concept of quasi-phase matching with artificially fabricated bulk structures. Both of these strategies allow the enhancement of parametric frequency conversion, such as second-order processes based on binary periodic poling of natural crystals, equivalent to a discrete phase change of the nonlinear polarization.

Nonlinear metamaterials allow nonlinear responses to be tailored through the engineering of their constituent elements and by providing novel degrees of freedom in the design of artificial materials with nontrivial nonlinear optical properties. Metasurfaces are two-dimensional planar structures that originate from the basic concepts of metamaterial physics. They introduce even broader possibilities via engineering arrays of optical resonators underpinning the emerging field of flat optics. As a result, metasurfaces do not require any phase-matching conditions, and their performance relies on the local enhancement of both electric and magnetic fields, so resonances play an essential role in the physics of nonlinear metasurfaces. Thus, nonlinear photonics of metasurfaces is driven in many cases by resonances in dielectric nanostructures: optically induced multipolar electric and magnetic Mie resonances, guided-mode resonances, and BICs. These resonances allow us to boost subwavelength confinement of local electromagnetic fields in dielectric nanostructures with high refractive index values, enhancing many effects in nonlinear photonics and offering novel opportunities for the subwavelength control of light at the nanoscale.

A significant challenge that remains is the relatively low values of the refractive index at the visible and near-IR frequencies. As mentioned recently [16], increasing the refractive index by a modest factor with modern methods of growth, fabrication, and subwavelength patterning will have a high impact on many applications of dielectric metasurfaces, including nonlinear photonics. In addition, the limited product of Q-factor and bandwidth restricts the utilization of ultrashort pulses for exciting strong nonlinear responses of ultrahigh-Q metasurfaces.

We have presented above some recent (mainly, over the last two years) developments in the field of nonlinear photonics of metasurfaces deviating from the traditional discussions of the SHG and THG with nonlinear metasurfaces and their conversion efficiencies [12,13,148,149]. In particular, we have emphasized multi-frequency effects, cascaded harmonic generation, asymmetric frequency conversion, and the nonlinear chiral response of metasurfaces. Most of the effects reported for nonlinear metasurfaces highlight the importance of the optically induced magnetic response of engineering nonmagnetic resonant structures for many applications in optics. In addition, we have discussed nonperturbative nonlinear regimes, which might introduce new design strategies in the field of nonlinear metasurfaces, and applications of nonlinear metasurfaces to quantum photonics, underpinning efficient flat-optics quantum metadevices.

Many novel directions in all-dielectric resonant photonics are expected to appear soon. One of these novel ideas is associated with the recently suggested concept of Mie voids. Indeed, Mie solutions are discussed usually for a sphere made of a high-index material with the refractive index n_1 being placed in a surrounding medium with lower refractive index n_2 (namely, $n_1 > n_2$). However, the opposite case is also possible, and we may consider low-index voids placed in high-index dielectric surrounding media ($n_1 < n_2$) [150]. Dielectric Mie voids can support localized optical modes, thus confining light in air. Importantly, these Mie void modes are not affected by loss and dispersion of the surrounding dielectric media [150]. They can be used for novel applications, as well as in combination with dielectric resonant nanoparticles and dielectric metasurfaces.

Current advances in tunable resonant nonlinear metasurfaces will allow us to achieve full all-optical control over the transient behavior of nonlinearities at femtosecond switching speeds. Recently, studies revealed the importance of temporal (femtosecond) responses of nonlinearities that will make metasurfaces very demanding for high-speed data processing. High-index semiconductor metasurfaces with rapidly tuned high-Q resonances enable a novel class of time-variant metasurfaces that allow the dynamic control of the nonlinear optical response in time-variant semiconductor metasurfaces supporting high-Q resonances [62]. Time-modulated metasurfaces can be employed for dynamic wavefront engineering and space-time photonics for the switching/tuning mechanisms providing the key to enable photonic technologies for the next generation of nanoscale pulse shapers, optical switches, and light sources [151].

Combining the advantages of all-dielectric metasurfaces with a resonant response would allow tunable control over the electromagnetic fields [152], also realizing novel types of chiral biosensors based on high-Q resonances, and thus increasing both device sensitivity and their multiplexing abilities. Modern integrated photonics requires developments in device design, material synthesis, nanofabrication, and characterization. The combination of these efforts can be realized with all-dielectric metasurface-based photonics underpinning new, not yet demonstrated applications. We envisage that many novel discoveries in all-dielectric resonant metaphotonics will be demonstrated in the coming years.

There are still many challenges to overcome. One important problem arises from the use of constituent materials. All-dielectric nanostructures are less lossy but show smaller values of nonlinear response, and their larger mode volumes due to the diffraction limit that increase the device footprints. Transparent oxides and two-dimensional materials have been successfully adopted as important materials to create hybrid metasurfaces [153]. For tunability, metasurface-based photonics needs to employ a combination of old and novel materials such as polymers, perovskites, TMDCs, and phase change materials [154]. This would enable diverse functionalities of metasystems and metasurfaces for efficient spatial and temporal control of light expanding applications of these concepts in nanolasers, tunable metadevices, metachemistry, and the design of a new generation of sensing devices.

We expect that more novel materials with distinguished nonlinearities at the nanoscale will emerge soon, and the recently emerged concepts of nonlinear metasurface photonics will find applications in the development of flexible electronic and optoelectronic devices, including nanolasers and detectors for miniaturized optical systems for holography, augmented reality, LIDAR, etc. We believe that we will soon witness many novel discoveries in this and related fields that are difficult to predict now and that the best in this field is yet to come.

Funding. Australian National University; Army Research Office (FA520921P0034); Australian Research Council (DP210101292).

Acknowledgment. The authors thank their colleagues from the Australian National University in Canberra, the National Institute of Standards and Technology in Gaithersburg, Sandia National Laboratories in Albuquerque, and the ITMO University in St. Petersburg for productive collaboration, continuous support, and insightful discussions, and also thank the editors of this special issue Thomas Pertsch, Guixin Li, Shumin Xiao, and Arka Majumdar for their critical reading of the initial version of this manuscript and useful suggestions. Support from the Australian Research Council, the Strategic Fund of the Australian National University, the International Technology Center Indo-Pacific (ITC IPAC) and Army Research Office is acknowledged. P.V. acknowledges support under the Professional Research Experience Program (PREP), funded by the National Institute of Standards and Technology and administered through the Department of Chemistry and Biochemistry, University of Maryland.

Disclosures. The authors declare no conflicts of interest.

Data Availability. No data were generated or analyzed in the presented research.

REFERENCES

1. A. Kildishev, A. Boltasseva, and V. Shalaev, "Planar photonics with metasurfaces," Science **339**, 1232009 (2013).
2. N. Yu and F. Capasso, "Flat optics with designer metasurfaces," Nat. Nanotechnol. **13**, 139–150 (2014).
3. P. Lalanne and P. Chavel, "Metalenses at visible wavelengths: past, present, perspectives," Laser Photon. Rev. **11**, 1600295 (2017).
4. H.-H. Hsiao, C.-H. Chu, and D.-P. Tsai, "Fundamentals and applications of metasurfaces," Small Methods **1**, 1600064 (2017).
5. C.-W. Qiu, T. Zhang, G. Hu, and Y. Kivshar, "Quo vadis, metasurfaces?" Nano Lett. **21**, 5461–5474 (2021).
6. A. Dorrah and F. Capasso, "Tunable structured light with flat optics," Science **376**, eabi6860 (2022).
7. A. Krasnok, M. Tymchenko, and A. Alu, "Nonlinear metasurfaces: a paradigm shift in nonlinear optics," Mater. Today **21**, 8–21 (2018).
8. T. Huang, X. Zhao, S. Zeng, A. Crunteanu, P. P. Shum, and N. Yu, "Planar nonlinear metasurface optics and their applications," Rep. Prog. Phys. **83**, 126101 (2020).
9. M. Kauranen and A. Zayats, "Nonlinear plasmonics," Nat. Photonics **6**, 737–748 (2012).
10. E. Rahimi and R. Gordon, "Nonlinear plasmonic metasurfaces," Adv. Opt. Mater. **6**, 1800274 (2018).
11. B. Sain, C. Meier, and T. Zentgraf, "Nonlinear optics in all-dielectric nanoantennas and metasurfaces: a review," Adv. Photon. **1**, 024002 (2019).
12. G. Grinblat, "Nonlinear dielectric nanoantennas and metasurfaces: frequency conversion and wavefront control," ACS Photon. **8**, 3406–3432 (2021).
13. T. Pertsch and Y. Kivshar, "Nonlinear optics with resonant metasurfaces," MRS Bull. **45**, 210–220 (2020).
14. Y. Kivshar, "The rise of Mie-tronics," Nano Lett. **22**, 3513–3515 (2022).
15. K. Koshelev, A. Bogdanov, and Y. Kivshar, "Meta-optics and bound states in the continuum," Sci. Bull. **64**, 836–842 (2019).
16. J. B. Khurgin, "Expanding the photonic palette: exploring high index materials," ACS Photon. **9**, 743–751 (2022).
17. S. Liu, P. P. Vabishchevich, A. Vaskin, J. L. Reno, G. A. Keeler, M. B. Sinclair, I. Staude, and I. Brener, "An all-dielectric metasurface as a broadband optical frequency mixer," Nat. Commun. **9**, 2507 (2018).
18. G. Sartorello, N. Olivier, J. Zhang, W. Yue, D. J. Gosztola, G. P. Wiederrecht, G. Wurtz, and A. V. Zayats, "Ultrafast optical modulation of second-and third-harmonic generation from cut-disk-based metasurfaces," ACS Photon. **3**, 1517–1522 (2016).
19. M. R. Shcherbakov, D. N. Neshev, B. Hopkins, A. S. Shorokhov, I. Staude, E. V. Melik-Gaykazyan, M. Decker, A. A. Ezhov, A. E. Miroshnichenko, I. Brener, A. A. Fedyanin, and Y. S. Kivshar, "Enhanced third-harmonic generation in silicon nanoparticles driven by magnetic response," Nano Lett. **14**, 6488–6492 (2014).
20. S. Liu, M. B. Sinclair, S. Saravi, G. A. Keeler, Y. Yang, J. Reno, G. M. Peake, F. Setzpfandt, I. Staude, T. Pertsch, and I. Brener, "Resonantly enhanced second-harmonic generation using III–V semiconductor all-dielectric metasurfaces," Nano Lett. **16**, 5426–5432 (2016).
21. S. Liu, A. Vaskin, S. Addamane, B. Leung, M.-C. Tsai, Y. Yang, P. P. Vabishchevich, G. A. Keeler, G. Wang, X. He, Y. Kim, N. F. Hartmann, H. Htoon, S. K. Doorn, M. Zilk, T. Pertsch, G. Balakrishnan, M. B. Sinclair, I. Staude, and I. Brener, "Light-emitting metasurfaces: simultaneous control of spontaneous emission and far-field radiation," Nano Lett. **18**, 6906–6914 (2018).
22. G. Grinblat, Y. Li, M. P. Nielsen, R. F. Oulton, and S. A. Maier, "Degenerate four-wave mixing in a multiresonant germanium nanodisk," ACS Photon. **4**, 2144–2149 (2017).
23. W. Tong, C. Gong, X. Liu, S. Yuan, Q. Huang, J. Xia, and Y. Wang, "Enhanced third harmonic generation in a silicon metasurface using trapped mode," Opt. Express **24**, 19661–19670 (2016).
24. M. R. Shcherbakov, K. Werner, Z. Fan, N. Talisa, E. Chowdhury, and G. Shvets, "Photon acceleration and tunable broadband harmonics generation in nonlinear time-dependent metasurfaces," Nat. Commun. **10**, 1 (2019).
25. K. I. Okhlopkov, A. Zilli, A. Tognazzi, D. Rocco, L. Fagiani, E. Mafakheri, M. Bollani, M. Finazzi, M. Celebrano, M. R. Shcherbakov, C. De Angelis, and A. A. Fedyanin, "Tailoring third-harmonic diffraction efficiency by hybrid modes in high-*Q* metasurfaces," Nano Lett. **21**, 10438–10445 (2021).
26. P. P. Vabishchevich, S. Liu, M. B. Sinclair, G. A. Keeler, G. M. Peake, and I. Brener, "Enhanced second-harmonic generation using broken symmetry III–V semiconductor Fano metasurfaces," ACS Photon. **5**, 1685–1690 (2018).
27. A. P. Anthur, H. Zhang, R. Paniagua-Dominguez, D. A. Kalashnikov, S. T. Ha, T. W. Maß, A. I. Kuznetsov, and L. Krivitsky, "Continuous wave second harmonic generation enabled by quasi-bound-states in the continuum on gallium phosphide metasurfaces," Nano Lett. **20**, 8745–8751 (2020).
28. Z. Liu, Y. Xu, Y. Lin, J. Xiang, T. Feng, Q. Cao, J. Li, S. Lan, and J. Liu, "High-*Q* quasibound states in the continuum for nonlinear metasurfaces," Phys. Rev. Lett. **123**, 253901 (2019).
29. G. Yang, S. U. Dev, M. S. Allen, J. W. Allen, and H. Harutyunyan, "Optical bound states in the continuum enabled by magnetic resonances coupled to a mirror," Nano Lett. **22**, 2001–2008 (2022).
30. K. Koshelev, S. Kruk, E. Melik-Gaykazyan, J.-H. Choi, A. Bogdanov, H.-G. Park, and Y. Kivshar, "Subwavelength dielectric resonators for nonlinear nanophotonics," Science **367**, 288–292 (2020).
31. K. Koshelev, S. Lepeshov, M. Liu, A. Bogdanov, and Y. Kivshar, "Asymmetric metasurfaces with high-*Q* resonances governed by bound states in the continuum," Phys. Rev. Lett. **121**, 193903 (2018).
32. J. Kühne, T. Weber, L. Kühner, J. Wang, S. A. Maier, and A. Tittl, "Fabrication tolerance impact on BIC metasurface resonances," in *European Conference on Lasers and Electro-Optics* (Optical Society of America, 2021), paper ck_p_2.

33. R. Camacho-Morales, L. Xu, H. Zhang, S. T. Ha, L. Krivitsky, A. I. Kuznetsov, M. Rahmani, and D. Neshev, "Sum-frequency generation in high-*Q* GaP metasurfaces driven by leaky-wave guided modes," Nano Lett. **22**, 6141–6148 (2022).
34. L. Kühner, L. Sortino, B. Tilmann, T. Weber, K. Watanabe, T. Taniguchi, S. A. Maier, and A. Tittl, "High-*Q* nanophotonics over the full visible spectrum enabled by hexagonal boron nitride metasurfaces," arXiv, arXiv:2210.11314 (2022).
35. R. Camacho-Morales, D. Rocco, L. Xu, V. F. Gili, N. Dimitrov, L. Stoyanov, Z. Ma, A. Komar, M. Lysevych, F. Karouta, A. A. Dreischuh, H. H. H. Tan, G. Leo, C. De Angelis, C. Jagadish, A. E. Miroshnichenko, M. Rahmani, and D. N. Neshev, "Infrared upconversion imaging in nonlinear metasurfaces," Adv. Photon. **3**, 036002 (2021).
36. L. Xu, D. A. Smirnova, R. Camacho-Morales, R. A. Aoni, K. Z. Kamali, M. Cai, C. Ying, Z. Zheng, A. E. Miroshnichenko, D. N. Neshev, and M. Rahmani, "Enhanced four-wave mixing from multi-resonant silicon Dimer-hole membrane metasurfaces," New J. Phys. **24**, 035002 (2022).
37. F. J. Löchner, A. N. Fedotova, S. Liu, G. A. Keeler, G. M. Peake, S. Saravi, M. R. Shcherbakov, S. Burger, A. A. Fedyanin, I. Brener, T. Pertsch, F. Setzpfandt, and I. Staude, "Polarization-dependent second harmonic diffraction from resonant GaAs metasurfaces," ACS Photon. **5**, 1786–1793 (2018).
38. M. J. Weber, *Handbook of Optical Materials* (CRC Press, 2018).
39. G. Marino, C. Gigli, D. Rocco, A. Lemaitre, I. Favero, C. De Angelis, and G. Leo, "Zero-order second harmonic generation from AlGaAs-on-insulator metasurfaces," ACS Photon. **6**, 1226–1231 (2019).
40. "Energy band gap EG of $Al_xGa_{1-x}As$ alloys," https://www.batop.de/information/eg_algaas.html.
41. M. Ohashi, T. Kondo, R. Ito, S. Fukatsu, Y. Shiraki, K. Kumata, and S. Kano, "Determination of quadratic nonlinear optical coefficient of Al_xGa_{1-x} as system by the method of reflected second harmonics," J. Appl. Phys. **74**, 596–601 (1993).
42. D. Khmelevskaia, D. Markina, V. Fedorov, G. Ermolaev, A. Arsenin, V. Volkov, A. Goltaev, Y. M. Zadiranov, I. Tzibizov, A. Pushkarev, A. K. Samusev, A. A. Shcherbakov, P. A. Belov, I. S. Mukhin, and S. V. Makarov, "Directly grown crystalline gallium phosphide on sapphire for nonlinear all-dielectric nanophotonics," Appl. Phys. Lett. **118**, 201101 (2021).
43. I. Shoji, T. Kondo, A. Kitamoto, M. Shirane, and R. Ito, "Absolute scale of second-order nonlinear-optical coefficients," J. Opt. Soc. Am. B **14**, 2268–2294 (1997).
44. F. Timpu, M. Reig Escalé, M. Timofeeva, N. Strkalj, M. Trassin, M. Fiebig, and R. Grange, "Enhanced nonlinear yield from barium titanate metasurface down to the near ultraviolet," Adv. Opt. Mater. **7**, 1900936 (2019).
45. S. Wemple, "Polarization fluctuations and the optical-absorption edge in $BaTiO_3$," Phys. Rev. B **2**, 2679–2689 (1970).
46. M. Semmlinger, M. L. Tseng, J. Yang, M. Zhang, C. Zhang, W.-Y. Tsai, D. P. Tsai, P. Nordlander, and N. J. Halas, "Vacuum ultraviolet light-generating metasurface," Nano Lett. **18**, 5738–5743 (2018).
47. A. Fedotova, M. Younesi, J. Sautter, A. Vaskin, F. J. Löchner, M. Steinert, R. Geiss, T. Pertsch, I. Staude, and F. Setzpfandt, "Second-harmonic generation in resonant nonlinear metasurfaces based on lithium niobate," Nano Lett. **20**, 8608–8614 (2020).
48. L. Carletti, A. Zilli, F. Moia, A. Toma, M. Finazzi, C. De Angelis, D. N. Neshev, and M. Celebrano, "Steering and encoding the polarization of the second harmonic in the visible with a monolithic $LiNbO_3$ metasurface," ACS Photon. **8**, 731–737 (2021).
49. M. Nauman, J. Yan, D. de Ceglia, M. Rahmani, K. Zangeneh Kamali, C. De Angelis, A. E. Miroshnichenko, Y. Lu, and D. N. Neshev, "Tunable unidirectional nonlinear emission from transition-metal-dichalcogenide metasurfaces," Nat. Commun. **12**, 5597 (2021).
50. A. A. Popkova, I. M. Antropov, G. I. Tselikov, G. A. Ermolaev, I. Ozerov, R. V. Kirtaev, S. M. Novikov, A. B. Evlyukhin, A. V. Arsenin, and V. O. Bessonov, "Nonlinear exciton-Mie coupling in transition metal dichalcogenide nanoresonators," Laser Photon. Rev. **16**, 2100604 (2022).
51. I. A. Rahman and A. Purqon, "First principles study of molybdenum disulfide electronic structure," J. Phys. Conf. Ser. **877**, 012026 (2017).
52. G. Cassabois, P. Valvin, and B. Gil, "Hexagonal boron nitride is an indirect bandgap semiconductor," Nat. Photonics **10**, 262–266 (2016).
53. J. Bar-David and U. Levy, "Nonlinear diffraction in asymmetric dielectric metasurfaces," Nano Lett. **19**, 1044–1051 (2019).
54. Y. Zhao, W. Jia, X.-J. Wang, Y. Dong, H.-H. Fang, Y. Yang, and H.-B. Sun, "Second-harmonic generation in strained silicon metasurfaces," Adv. Photon. Res. 2200157 (2022).
55. A. Garcia-Barrientos, J. L. Bernal-Ponce, J. Plaza-Castillo, A. Cuevas-Salgado, A. Medina-Flores, M. S. Garcia-Monterrosas, and A. Torres-Jacome, "Analysis, synthesis and characterization of thin films of a-Si:H (n-type and p-type) deposited by PECVD for solar cell applications," Materials **14**, 6349 (2021).
56. L. Xu, K. Zangeneh Kamali, L. Huang, M. Rahmani, A. Smirnov, R. Camacho-Morales, Y. Ma, G. Zhang, M. Woolley, D. Neshev, and A. E. Miroshnichenko, "Dynamic nonlinear image tuning through magnetic dipole quasi-BIC ultrathin resonators," Adv. Sci. **6**, 1802119 (2019).
57. T. D. Gupta, L. Martin-Monier, J. Butet, K.-Y. Yang, A. Leber, C. Dong, T. Nguyen-Dang, W. Yan, O. J. Martin, and F. Sorin, "Second harmonic generation in glass-based metasurfaces using tailored surface lattice resonances," Nanophotonics **10**, 3465–3475 (2021).
58. A. Bhatnagar, K. V. Reddy, and V. Srivastava, "Optical energy gap of amorphous selenium: effect of annealing," J. Phys. D **18**, L149 (1985).
59. F. Yue, R. Piccoli, M. Y. Shalaginov, T. Gu, K. A. Richardson, R. Morandotti, J. Hu, and L. Razzari, "Nonlinear mid-infrared metasurface based on a phase-change material," Laser Photon. Rev. **15**, 2000373 (2021).
60. Y. Zhang, J. B. Chou, J. Li, H. Li, Q. Du, A. Yadav, S. Zhou, M. Y. Shalaginov, Z. Fang, and H. Zhong, "Broadband transparent optical phase change materials for high-performance nonvolatile photonics," Nat. Commun. **10**, 4279 (2019).
61. H. Zhang, X. Wang, and W. Zhang, "First-principles investigation of amorphous Ge-Sb-Se-Te optical phase-change materials," Opt. Mater. Express **12**, 2497–2506 (2022).
62. V. V. Zubyuk, P. A. Shafirin, M. R. Shcherbakov, G. Shvets, and A. A. Fedyanin, "Externally driven nonlinear time-variant metasurfaces," ACS Photon. **9**, 493–502 (2022).
63. G. Grinblat, Y. Li, M. P. Nielsen, R. F. Oulton, and S. A. Maier, "Enhanced third harmonic generation in single germanium nanodisks excited at the anapole mode," Nano Lett. **16**, 4635–4640 (2016).
64. G. Connell, R. Temkin, and W. Paul, "Amorphous germanium III. Optical properties," Adv. Phys. **22**, 643–665 (1973).
65. N. K. Hon, R. Soref, and B. Jalali, "The third-order nonlinear optical coefficients of Si, Ge, and $Si_{1-x}Ge_x$ in the midwave and longwave infrared," J. Appl. Phys. **110**, 011301 (2011).
66. Y. Gao, Y. Fan, W. Wang, Y. Yang, Q. Song, and S. Xiao, "Nonlinear holographic all-dielectric metasurfaces," Nano Lett. **18**, 8054–8061 (2018).
67. Y. Yang, W. Wang, A. Boulesbaa, I. I. Kravchenko, D. P. Briggs, A. Puretzky, D. Geohegan, and J. Valentine, "Nonlinear Fano-resonant dielectric metasurfaces," Nano Lett. **15**, 7388–7393 (2015).
68. R. Woodward, R. Murray, C. Phelan, R. De Oliveira, T. Runcorn, E. Kelleher, S. Li, E. De Oliveira, G. Fechine, G. Eda, and C. J. S. de Matos, "Characterization of the second-and third-order nonlinear optical susceptibilities of monolayer MoS_2 using multiphoton microscopy," 2D Mater. **4**, 011006 (2016).
69. S. Wu, "Line shape analysis of higher order nonlinear processes in time-resolved degenerate four-wave mixing in GaAs," J. Appl. Phys. **73**, 8035–8040 (1993).
70. A. S. Shorokhov, E. V. Melik-Gaykazyan, D. A. Smirnova, B. Hopkins, K. E. Chong, D.-Y. Choi, M. R. Shcherbakov, A. E. Miroshnichenko, D. N. Neshev, A. A. Fedyanin, and Y. S. Kivshar, "Multifold enhancement of third-harmonic generation in dielectric nanoparticles driven by magnetic Fano resonances," Nano Lett. **16**, 4857–4861 (2016).
71. L. Xu, M. Rahmani, Y. Ma, D. A. Smirnova, K. Z. Kamali, F. Deng, Y. K. Chiang, L. Huang, H. Zhang, S. Gould, D. N. Neshev, and A. E. Miroshnichenko, "Enhanced light–matter interactions in dielectric nanostructures via machine-learning approach," Adv. Photon. **2**, 026003 (2020).

72. K. Narayanan and S. F. Preble, "Optical nonlinearities in hydrogenated-amorphous silicon waveguides," Opt. Express **18**, 8998–9005 (2010).
73. J. Gao, M. A. Vincenti, J. Frantz, A. Clabeau, X. Qiao, L. Feng, M. Scalora, and N. M. Litchinitser, "Near-infrared to ultra-violet frequency conversion in chalcogenide metasurfaces," Nat. Commun. **12**, 1 (2021).
74. T. Wang, X. Gai, W. Wei, R. Wang, Z. Yang, X. Shen, S. Madden, and B. Luther-Davies, "Systematic Z-scan measurements of the third order nonlinearity of chalcogenide glasses," Opt. Mater. Express **4**, 1011–1022 (2014).
75. M. Semmlinger, M. Zhang, M. L. Tseng, T.-T. Huang, J. Yang, D. P. Tsai, P. Nordlander, and N. J. Halas, "Generating third harmonic vacuum ultraviolet light with a TiO_2 metasurface," Nano Lett. **19**, 8972–8978 (2019).
76. T. Hashimoto, T. Yoko, and S. Sakka, "Sol–gel preparation and third-order nonlinear optical properties of TiO_2 thin films," Bull. Chem. Soc. Jpn. **67**, 653–660 (1994).
77. R. Camacho-Morales, M. Rahmani, S. Kruk, L. Wang, L. Xu, D. A. Smirnova, A. S. Solntsev, A. Miroshnichenko, H. H. Tan, F. Karouta, S. Naureen, K. Vora, L. Carletti, C. De Angelis, C. Jagadish, Y. S. Kivshar, and D. N. Neshev, "Nonlinear generation of vector beams from AlGaAs nanoantennas," Nano Lett. **16**, 7191–7197 (2016).
78. S. S. Kruk, R. Camacho-Morales, L. Xu, M. Rahmani, D. A. Smirnova, L. Wang, H. H. Tan, C. Jagadish, D. N. Neshev, and Y. S. Kivshar, "Nonlinear optical magnetism revealed by second-harmonic generation in nanoantennas," Nano Lett. **17**, 3914–3918 (2017).
79. A. Fedotova, L. Carletti, A. Zilli, F. Setzpfandt, I. Staude, A. Toma, M. Finazzi, C. De Angelis, T. Pertsch, D. N. Neshev, and M. Celebrano, "Lithium niobate meta-optics," ACS Photon. **9**, 3745–3763 (2022).
80. M. L. Tseng, M. Semmlinger, and M. Zhang, "Vacuum ultraviolet nonlinear metalens," Sci. Adv. **8**, eabn5644 (2022).
81. S. D. Gennaro, C. F. Doiron, N. Karl, P. P. Iyer, D. K. Serkland, M. B. Sinclair, and I. Brener, "Cascaded optical nonlinearities in dielectric metasurfaces," ACS Photon. **9**, 1026–1032 (2022).
82. G. Marino, D. Rocco, C. Gigli, G. Beaudoin, K. Pantzas, S. Suffit, P. Filloux, I. Sagnes, G. Leo, and C. De Angelis, "Harmonic generation with multi-layer dielectric metasurfaces," Nanophotonics **10**, 1837–1843 (2021).
83. N. Kumar, S. Najmaei, Q. Cui, F. Ceballos, P. M. Ajayan, J. Lou, and H. Zhao, "Second harmonic microscopy of monolayer MoS_2," Phys. Rev. B **87**, 161403 (2013).
84. L. M. Malard, T. V. Alencar, A. P. M. Barboza, K. F. Mak, and A. M. De Paula, "Observation of intense second harmonic generation from MoS_2 atomic crystals," Phys. Rev. B **87**, 201401 (2013).
85. G. Wang, X. Marie, I. Gerber, T. Amand, D. Lagarde, L. Bouet, M. Vidal, A. Balocchi, and B. Urbaszek, "Giant enhancement of the optical second-harmonic emission of WSe_2 monolayers by laser excitation at exciton resonances," Phys. Rev. Lett. **114**, 097403 (2015).
86. M. Zhu, S. Abdollahramezani, C. Li, T. Fan, H. Harutyunyan, and A. Adibi, "Dynamically tunable second-harmonic generation using hybrid nanostructures incorporating phase-change chalcogenides," Nanophotonics **11**, 2727–2735 (2022).
87. E. Fazio, F. Pettazzi, M. Centini, M. Chauvet, A. Belardini, M. Alonzo, C. Sibilia, M. Bertolotti, and M. Scalora, "Complete spatial and temporal locking in phase-mismatched second-harmonic generation," Opt. Express **17**, 3141–3147 (2009).
88. M. Centini, V. Roppo, E. Fazio, F. Pettazzi, C. Sibilia, J. W. Haus, J. V. Foreman, N. Akozbek, M. J. Bloemer, and M. Scalora, "Inhibition of linear absorption in opaque materials using phase-locked harmonic generation," Phys. Rev. Lett. **101**, 113905 (2008).
89. A. Leitis, A. Tittl, M. Liu, B. H. Lee, M. B. Gu, Y. S. Kivshar, and H. Altug, "Angle-multiplexed all-dielectric metasurfaces for broadband molecular fingerprint retrieval," Sci. Adv. **5**, eaaw2871 (2019).
90. M. R. Shcherbakov, P. Shafirin, and G. Shvets, "Overcoming the efficiency-bandwidth tradeoff for optical harmonics generation using nonlinear time-variant resonators," Phys. Rev. A **100**, 063847 (2019).
91. M. Vincenti, J. Gao, D. de Ceglia, J. Frantz, M. Scalora, and N. Litchinitser, "Stacked chalcogenide metasurfaces for third harmonic generation in the UV range," New J. Phys. **24**, 035005 (2022).
92. H. Weigand, V. V. Vogler-Neuling, M. R. Escalé, D. Pohl, F. U. Richter, A. Karvounis, F. Timpu, and R. Grange, "Enhanced electro-optic modulation in resonant metasurfaces of lithium niobate," ACS Photon. **8**, 3004–3009 (2021).
93. A. Weiss, C. Frydendahl, J. Bar-David, R. Zektzer, E. Edrei, J. Engelberg, N. Mazurski, B. Desiatov, and U. Levy, "Tunable metasurface using thin-film lithium niobate in the telecom regime," ACS Photon. **9**, 605–612 (2022).
94. J. Gao, M. A. Vincenti, J. Frantz, A. Clabeau, X. Qiao, L. Feng, M. Scalora, and N. M. Litchinitser, "All-optical tunable wavelength conversion in opaque nonlinear nanostructures," Nanophotonics **11**, 4027–4035 (2022).
95. Q. Yuan, L. Fang, H. Fang, J. Li, T. Wang, W. Jie, J. Zhao, and X. Gan, "Second harmonic and sum-frequency generations from a silicon metasurface integrated with a two-dimensional material," ACS Photon. **6**, 2252–2259 (2019).
96. J. Deka, M. Dandu, L. K. As, S. Menon, K. Jyothsna, R. Biswas, K. Majumdar, and V. Raghunathan, "Polarization independent enhancement of zeroth order diffracted second harmonic from multilayer gallium selenide on a silicon resonant metasurface," Opt. Express **28**, 35695–35707 (2020).
97. F. J. Löchner, A. George, K. Koshelev, T. Bucher, E. Najafidehaghani, A. Fedotova, D.-Y. Choi, T. Pertsch, I. Staude, Y. Kivshar, A. Turchanin, and F. Setzpfandt, "Hybrid dielectric metasurfaces for enhancing second-harmonic generation in chemical vapor deposition grown MoS_2 monolayers," ACS Photon. **8**, 218–227 (2020).
98. N. Bernhardt, K. Koshelev, S. J. White, K. W. C. Meng, J. E. Froch, S. Kim, T. T. Tran, D.-Y. Choi, Y. Kivshar, and A. S. Solntsev, "Quasi-BIC resonant enhancement of second-harmonic generation in WS_2 monolayers," Nano Lett. **20**, 5309–5314 (2020).
99. Z. Liu, J. Wang, B. Chen, Y. Wei, W. Liu, and J. Liu, "Giant enhancement of continuous wave second harmonic generation from few-layer GaSe coupled to high-*Q* quasi bound states in the continuum," Nano Lett. **21**, 7405–7410 (2021).
100. S. Liu, G. A. Keeler, J. L. Reno, M. B. Sinclair, and I. Brener, "III–V semiconductor nanoresonators—a new strategy for passive, active, and nonlinear all-dielectric metamaterials," Adv. Opt. Mater. **4**, 1457–1462 (2016).
101. S. D. Gennaro, M. Goldflam, D. B. Burckel, J. Jeong, M. B. Sinclair, and I. Brener, "Dielectric metasurfaces made from vertically oriented nanoresonators," J. Opt. Soc. Am. B **38**, C33–C41 (2021).
102. C. Schlickriede, S. Kruk, L. Wang, B. Sain, Y. Kivshar, and T. Zentgraf, "Nonlinear imaging with all-dielectric metasurfaces," Nano Lett. **20**, 4370–4376 (2020).
103. S. Kruk, L. Wang, B. Sain, Z. Dong, J. Yang, T. Zentgraf, and Y. Kivshar, "Asymmetric parametric generation of images with nonlinear dielectric metasurfaces," Nat. Photonics **16**, 561–565 (2022).
104. C. Caloz, A. Alu, S. Tretyakov, D. Sounas, K. Achouri, and Z. Deck-Léger, "Electromagnetic nonreciprocity," Phys. Rev. Appl. **10**, 047001 (2018).
105. A. M. Mahmoud, A. R. Davoyan, and N. Engheta, "All-passive nonreciprocal metastructure," Nat. Commun. **6**, 8359 (2015).
106. N. Shitrit, J. Kim, D. Barth, H. Ramezani, Y. Wang, and X. Zhang, "Asymmetric free-space light transport at nonlinear metasurfaces," Phys. Rev. Lett. **121**, 046101 (2018).
107. R. Alaee, M. Albooyeh, A. Rahimzadegan, M. Mirmoosa, Y. Kivshar, and C. Rockstuhl, "All-dielectric reciprocal bianisotropic nanoparticles," Phys. Rev. B **92**, 245130 (2015).
108. M. Odit, P. Kapitanova, R. Belov, P. Alaee, C. Rockstuhl, and Y. Kivshar, "Experimental realisation of all-dielectric bianisotropic metasurfaces," Appl. Phys. Lett. **108**, 221903 (2016).
109. E. Mobini, R. Alaee, R. Boyd, and K. Dolgaleva, "Giant asymmetric second-harmonic generation in bianisotropic metasurfaces based on bound states in the continuum," ACS Photon. **8**, 3234–3240 (2021).
110. C. Argyropoulos, "Asymmetric control of light at the nanoscale," Nat. Photonics **16**, 556–557 (2022).

111. D. Sounas and A. Alu, "Fundamental bounds on the operation of Fano nonlinear isolators," Phys. Rev. B **97**, 115431 (2018).
112. M. Lawrence, D. Barton, and J. Dionne, "Nonreciprocal flat optics with silicon metasurfaces," Nano Lett. **18**, 1104–1109 (2018).
113. M. Cotrufo, A. Cordano, A. Polman, and A. Alu, "Nonlinearity-induced nonreciprocity in passive silicon gratings supporting quasi-bound states in the continuum," arXiv, arXiv:2210.05586 (2022).
114. M. Schäferling, D. Dregely, M. Hentschel, and H. Giessen, "Tailoring enhanced optical chirality: design principles for chiral plasmonic nanostructures," Phys. Rev. X **2**, 031010 (2012).
115. M. Gorkunov, A. Antonov, and Y. Kivshar, "Metasurfaces with maximum chirality empowered by bound states in the continuum," Phys. Rev. Lett. **125**, 093903 (2020).
116. T. Shi, Z.-L. Deng, G. Geng, X. Zeng, Y. Zeng, G. Hu, A. Overvig, J. Li, C.-W. Qiu, A. Alù, Y. S. Kivshar, and X. Li, "Planar chiral metasurfaces with maximal and tunable chiroptical response driven by bound states in the continuum," Nat. Commun. **13**, 4111 (2022).
117. D. Hooper, A. Mark, C. Kuppe, J. Collins, P. Fischer, and V. Valev, "Strong rotational anisotropies affect nonlinear chiral metamaterials," Adv. Mater. **29**, 1605110 (2017).
118. K. Koshelev, Y. Tang, Z. Hu, I. Kravchenko, G. Li, and Y. Kivshar, "Enhanced nonlinear circular dichroism in resonant dielectric metasurfaces," arXiv, arXiv:2202.12041 (2022).
119. K. Frizyuk, E. Melik-Gaykazyan, J.-H. Choi, M. Petrov, H.-G. Park, and Y. Kivshar, "Nonlinear circular dichroism in Mie-resonant nanoparticle dimers," Nano Lett. **21**, 4381–4387 (2021).
120. V. Zubyuk, L. Carletti, M. Shcherbakov, and S. Kruk, "Resonant dielectric metasurfaces in strong optical fields," APL Mater. **9**, 060701 (2021).
121. I. Sinev, K. Koshelev, Z. Liu, A. Rudenko, K. Ladutenko, A. Shcherbakov, Z. Sadrieva, M. Baranov, T. Itina, J. Liu, A. Bogdanov, and Y. Kivshar, "Observation of ultrafast self-action effects in quasi-BIC resonant metasurfaces," Nano Lett. **21**, 8848–8855 (2021).
122. G. Zograf, K. Koshelev, A. Zalogina, V. Korolev, R. Hollinger, D.-Y. Choi, M. Zuerch, C. Spielmann, B. Luther-Davies, D. Kartashov, S. Makarov, S. Kruk, and Y. Kivshar, "High-harmonic generation from resonant dielectric metasurfaces empowered by bound states in the continuum," ACS Photon. **9**, 567–574 (2022).
123. M. Shcherbakov, H. Zhang, M. Tripepi, G. Sartorello, N. Talisa, A. AlShafey, Z. Fan, J. Twardowski, L. Krivitsky, A. Kuznetsov, E. Chowdhury, and G. Shvets, "Generation of even and odd high harmonics in resonant metasurfaces using single and multiple ultra-intense laser pulses," Nat. Commun. **12**, 418 (2021).
124. P. Xia, C. Kim, F. Lu, T. Kanai, H. Akiyama, J. Itatani, and N. Ishii, "Nonlinear propagation effects in high harmonic generation in reflection and transmission from gallium arsenide," Opt. Express **26**, 29393–29400 (2018).
125. S. Jiang, J. Chen, H. Wei, C. Yu, and R. Lu, "Role of the transition dipole amplitude and phase on the generation of odd and even high-order harmonics in crystals," Phys. Rev. Lett. **120**, 253201 (2018).
126. S. Jiang, S. Gholam-Mirzaei, E. Crites, J. Beetar, M. Singh, R. Lu, M. Chini, and C. Lin, "Crystal symmetry and polarization of high-order harmonics in ZnO," J. Phys. B **52**, 225601 (2019).
127. K. Kaneshima, Y. Shinohara, K. Takeuchi, N. Ishii, K. Imasaka, T. Kaji, S. Ashihara, and K. Ishikawa, "Polarization-resolved study of high harmonics from bulk semiconductors," Phys. Rev. Lett. **120**, 243903 (2018).
128. U. Huttner, M. Kira, and S. Koch, "Ultrahigh off-resonant field effects in semiconductors," Laser Photon. Rev. **11**, 1700049 (2017).
129. S. Ghimire, A. DiChiara, E. Sistrunk, P. Agostini, L. DiMauro, and D. Reis, "Observation of high-order harmonic generation in a bulk crystal," Nat. Phys. **7**, 138–141 (2011).
130. C. Yu, S. Jiang, and R. Lu, "High order harmonic generation in solids: a review on recent numerical methods," Adv. Phys. X **4**, 1562982 (2019).
131. A. Rudenko, private communications (2022).
132. S. Xiao, M. Qin, J. Duan, F. Wu, and T. Liu, "Polarization-controlled dynamically switchable high-harmonic generation from all-dielectric metasurfaces governed by dual bound states in the continuum," Phys. Rev. B **105**, 195440 (2022).
133. S. Xiao, M. Qin, J. Duan, and T. Liu, "Robust enhancement of high-harmonic generation from all-dielectric metasurfaces enabled by polarisation-insensitive bound states in the continuum," Opt. Express **30**, 32590–32599 (2022).
134. P. Shafirin, V. Zubyuk, and M. Shcherbakov, "Nonlinear response of *Q*-boosting metasurfaces beyond the time-bandwidth limit," Nanophotonics **11**, 4053–4061 (2022).
135. A. S. Solntsev, G. S. Agarwal, and Y. S. Kivshar, "Metasurfaces for quantum photonics," Nat. Photonics **15**, 327–336 (2021).
136. K. Wang, M. Chekhova, and Y. Kivshar, "Metasurfaces for quantum technologies," Phys. Today **75**, 38–44 (2022).
137. D. Magde and H. Mahr, "Study in ammonium dihydrogen phosphate of spontaneous parametric interaction tunable from 4400 to 16000 Å," Phys. Rev. Lett. **18**, 905–907 (1967).
138. M. Parry, A. Mazzanti, A. Poddubny, G. Della Valle, D. N. Neshev, and A. A. Sukhorukov, "Enhanced generation of nondegenerate photon pairs in nonlinear metasurfaces," Adv. Photon. **3**, 055001 (2021).
139. A. Mazzanti, M. Parry, A. N. Poddubny, G. Della Valle, D. N. Neshev, and A. A. Sukhorukov, "Enhanced generation of angle correlated photon-pairs in nonlinear metasurfaces," New J. Phys. **24**, 035006 (2022).
140. G. Marino, A. S. Solntsev, L. Xu, V. F. Gili, L. Carletti, A. N. Poddubny, M. Rahmani, D. A. Smirnova, H. Chen, and A. Lematre, "Spontaneous photon-pair generation from a dielectric nanoantenna," Optica **6**, 1416–1422 (2019).
141. T. Santiago-Cruz, A. Fedotova, V. Sultanov, M. A. Weissflog, D. Arslan, M. Younesi, T. Pertsch, I. Staude, F. Setzpfandt, and M. Chekhova, "Photon pairs from resonant metasurfaces," Nano Lett. **21**, 4423–4429 (2021).
142. T. Santiago-Cruz, S. D. Gennaro, O. Mitrofanov, S. Addamane, J. Reno, I. Brener, and M. V. Chekhova, "Resonant metasurfaces for generating complex quantum states," Science **377**, 991–995 (2022).
143. J. Zhang, J. Ma, M. Parry, M. Cai, R. C. Morales, L. Xu, D. N. Neshev, and A. A. Sukhorukov, "Spatially entangled photon pairs from lithium niobate nonlocal metasurfaces," Sci. Adv. **8**, eabq4240 (2022).
144. L. Li, Z. Liu, X. Ren, S. Wang, V.-C. Su, M.-K. Chen, C. H. Chu, H. Y. Kuo, B. Liu, W. Zang, G. Guo, L. Zhang, Z. Wang, and S. Zhu, "Metalens-array–based high-dimensional and multiphoton quantum source," Science **368**, 1487–1490 (2020).
145. Y.-J. Gao, Z. Wang, R.-W. Jiang, Y. Peng, Z.-Y. Wang, D.-X. Qi, R.-H. Fan, W.-J. Tang, and M. Wang, "Multichannel distribution and transformation of entangled photons with dielectric metasurfaces," Phys. Rev. Lett. **129**, 023601 (2022).
146. D. Zhang, Y. Chen, S. Gong, W. Wu, W. Cai, M. Ren, X. Ren, S. Zhang, G. Guo, and J. Xu, "All-optical modulation of quantum states by nonlinear metasurface," Light Sci. Appl. **11**, 58 (2022).
147. V. Sultanov, T. Santiago-Cruz, and M. Chekhova, "Broadband polarization-tunable photon pairs from an ultrathin nonlinear film," arXiv, arXiv:2201.09517 (2022).
148. C. Wang, Y. Wen, J. Sun, and J. Zhou, "Recent progress on optical frequency conversion in nonlinear metasurfaces and nanophotonics," ES Mater. Manuf. **17**, 1–13 (2022).
149. G. Gigli and G. Leo, "All-dielectric $\chi^{(2)}$ metasurfaces: recent progress," Opto-Electron. Adv. **5**, 210093 (2022).
150. M. Hentschel, K. Koshelev, F. Sterl, S. Both, J. Karst, T. Weiss, Y. Kivshar, and H. Giessen, "Dielectric Mie voids: confining light in air," arXiv, arXiv:2205.07729 (2022).
151. E. Mikheeva, C. Kyrou, F. Bentata, S. Khadir, S. Cueff, and P. Genevet, "Space and time modulations of light with metasurfaces: recent progress and future prospects," ACS Photon. **9**, 1458–1482 (2022).
152. M. Ren, W. Cai, and J. Xu, "Tailorable dynamics in nonlinear optical metasurfaces," Adv. Mater. **32**, 1806317 (2020).
153. J. Guan, J.-E. Park, S. Deng, M. Tan, J. Hu, and T. Odom, "Light-matter interactions in hybrid material metasurfaces," Chem. Rev. **122**, 15177–15203 (2022).
154. P. Tonkaev, I. Sinev, M. Rybin, S. Makarov, and Y. Kivshar, "Multifunctional and transformative metaphotonics with emerging materials," Chem. Rev. **122**, 15414–15449 (2022).